Original Article
International Journal of Fuzzy Logic and Intelligent Systems
Vol. 13, No. 4, December 2013, pp. 324-335
http://dx.doi.org/10.5391/IJFIS.2013.13.4.324

ISSN(Print) 1598-2645
ISSN(Online) 2093-744X

Design, Control, and Implementation of Small Quad-Rotor System Under Practical Limitation of Cost Effectiveness

Seungho Jeong and Seul Jung
The Intelligent Systems and Emotional Engineering Laboratory, Department of Mechatronics Engineering, Chungnam National University, Daejeon, Korea

Abstract

This article presents the design, control, and implementation of a small quad-rotor system under the practical limitation of being cost effective for private use, such as in the cases of control education or hobbies involving radio-controlled systems. Several practical problems associated with implementing a small quad-rotor system had to be taken into account to satisfy this cost constraint. First, the size was reduced to attain better maneuverability. Second, the main control hardware was limited to an 8-bit processor such as an AVR to reduce cost. Third, the algorithms related to the control and sensing tasks were optimized to be within the computational capabilities of the available processor within one sampling time. A small quad-rotor system was ultimately implemented after satisfying all of the above practical limitations. Experimental studies were conducted to confirm the control performance and the operational abilities of the system.

Keywords: Quad-rotor system, Hardware limitation, Optimized design, Cost constraint

1. Introduction

There has been increasing research into the development of unmanned vehicle systems (UVS) that will help save human labor or even human lives in dangerous environments. A successful UVS must feature several technologies, including localization, path planning, and control, if it is to be autonomous [1-4].

Typically, in unmanned aerial vehicle (UAV) systems, autonomous navigation plays an important role in gathering information from the ground [5]. Particularly for military operations in dangerous zones, UAVs undertake a variety of valuable missions such as surveillance, monitoring, and even defense. Most military UAVs adopt a conventional take-off and landing design that requires a long range and a wide and long runway to take off and land.

However, surveillance in complex environments such as urban areas requires a different take-off and landing approach. UAVs need to be capable of vertical take-off and landing in a limited space [6, 7].

Recently, the use of fan-type power has attracted the attention of researchers developing small UAVs for taking off and landing in confined areas. Instead of using a single propeller, four equal-sized fans are utilized. Since such a "quad-rotor" system has four equal-sized fans, it can generate a greater amount of thrust and thus realize more stable hovering control.

Received: Sep. 12, 2013
Revised : Dec. 16, 2013
Accepted: Dec. 25, 2013

Correspondence to: Seul Jung
(jungs@cnu.ac.kr)

Although quad-rotor systems are affected by wind and suffer from limited battery capacity when operating in an outdoor environment, these systems have attracted researcher's attention owing to their apparent suitability for performing certain tasks. Such tasks include traffic monitoring on highways and the surveillance of accidents on the road.

Considerable research has been undertaken into the development of quad-rotor systems. Quad-rotor systems have already been applied to surveillance tasks [8-18], and aggressive maneuvering control has also been implemented [19]. Excellent maneuvering control has been demonstrated for small quad-rotors developed at the University of Pennsylvania. While most quad-rotor systems focus on flying, Flymobile focuses on both flying and driving, and we have performed successful flying and driving tests [20, 21]. Recent research into quad-rotor systems has focused more on localization based on sensors [22-24].

In this study, a novel design was developed for small quad-rotor systems meant for private use such as control education or hobbies involving radio-controlled systems, with the goal of producing a smaller, cost-effective unit. Another reason for downsizing the system was to improve the maneuverability of the quad-rotor system. Its small size allows high speed and rapid changes in direction to increase its mobility.

Since the quad-rotor system is small, there are several practical limitations affecting the implementation of the system at a price point that is affordable for public use. However, the reduction of cost involves several technical constraints:

1) The structural size is reduced to attain better maneuverability. The mass is less than 1 kg, and the length is 0.5 m.
2) The control hardware is limited to an 8-bit processor such as an AVR, rather than a digital signal processor (DSP) chip. Some mathematical functions such as square root and arctangent must be approximated since they are beyond the capabilities of 8-bit processors.
3) Algorithms related to the control and sensing processes must be shortened in order to minimize the calculation time in line with the sampling time for practical control.
4) Integer-based operations are required for numerical calculations.

After compensating for the aforementioned problems, we actually implemented a small quad-rotor system. Experimental studies of several flying tests in both indoor and outdoor environments were conducted to demonstrate the operational abilities of the system.

Table 1. Motion attained by controlling rotor speed

	Front rotor F_F	Right rotor F_R	Back rotor F_B	Left rotor F_L
Move up	⇑	⇑	⇑	⇑
Stationary	↑	↑	↑	↑
Move down	ˆ	ˆ	ˆ	ˆ
Move forward	ˆ	↑	⇑	↑
Move backward	⇑	↑	ˆ	↑
Move left	↑	⇑	↑	ˆ
Move right	↑	ˆ	↑	⇑
Turn right	ˆ	⇑	ˆ	⇑
Turn left	⇑	ˆ	⇑	ˆ

(Relative scale :⇑>↑>ˆ)

2. Quad-Rotor System

2.1 Kinematics

The quad-rotor system has four rotors and propellers, as shown in Figure 1. A pair of propellers rotates in the clockwise direction (F_R, F_L) and another pair (F_F, F_B) rotates in the counter-clockwise direction to prevent spinning of the body. Combining the force F_i generated by each of the propellers determines the motion of the system. Table 1 shows the motion based on the induced thrust forces where F_F, F_B, F_R, F_L are the forces produced by the front, back, right, and left rotors, respectively.

The coordinates of the quad-rotor system $(O_V X_V Y_V Z_V)$ are defined in the global coordinate$(O_W X_W Y_W Z_W)$.

Changing the speed of each rotor generates translational movement $P = [x, y, z]^T$ and rotational movement $\Omega = [\phi, \theta, \psi]^T$. Note that the linear velocity and the angular velocity in the global frame are defined as

$$V = \dot{P} = \begin{bmatrix} \dot{x} \\ \dot{y} \\ \dot{z} \end{bmatrix}, \quad \omega = \dot{\Omega} = \begin{bmatrix} \dot{\phi} \\ \dot{\theta} \\ \dot{\psi} \end{bmatrix} \tag{1}$$

where ϕ, θ, ψ are the roll, pitch, and yaw angles, respectively.

The linear velocity V is related to the linear velocity of the vehicle frame V_V through a rotational transformation as

$$V = RV_V \tag{2}$$

where $R(\phi, \theta, \psi) = R_{(Z_W,\psi)} R_{(Y_W,\theta)} R_{(X_W,\phi)}$ is the resultant

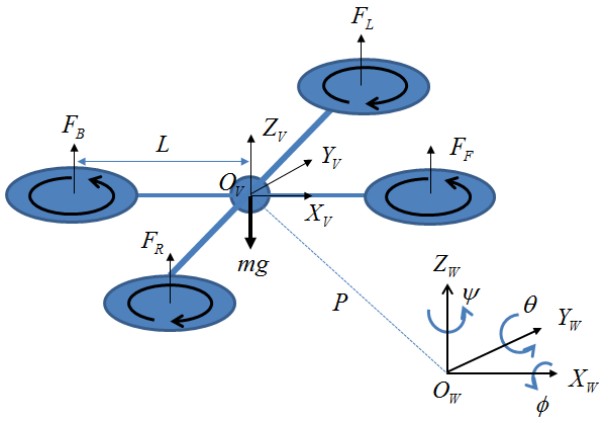

Figure 1. Model of a quad-rotor system.

rotational matrix for the roll, pitch, and yaw rotation about global coordinates X_W, Y_W, Z_W, respectively. It is found as

$$R = \begin{bmatrix} c\theta c\psi & s\phi s\theta c\psi - c\phi s\psi & c\phi s\theta c\psi + s\phi s\psi \\ c\theta s\psi & s\phi s\theta s\psi + c\phi c\psi & c\phi s\theta s\psi - s\phi c\psi \\ -s\theta & s\phi c\theta & c\phi c\theta \end{bmatrix} \quad (3)$$

where $c\phi = \cos(\phi)$, $s\phi = \sin(\phi)$, $c\theta = \cos(\theta)$, $s\theta = \sin(\theta)$, and $c\psi = \cos(\psi)$, $s\psi = \sin(\psi)$.

Therefore, the linear velocity in the vehicle coordinate is found to be

$$V_V = \begin{bmatrix} u \\ v \\ w \end{bmatrix} = R^T V \quad (4)$$

where $R^{-1} = R^T$ and u, v, w are the linear velocity about the X_V, Y_V, Z_V axis, respectively.

The angular velocity is given by

$$\omega = T\omega_V \quad (5)$$

where ω_V is the angular velocity of the vehicle frame, and T is the Euler kinematic equation and defined by

$$T = \begin{bmatrix} 1 & \sin(\phi)\tan(\theta) & \cos(\phi)\tan(\theta) \\ 0 & \cos(\phi) & -\sin(\phi) \\ 0 & \sin(\phi)/\cos(\theta) & \cos(\phi)/\cos(\theta) \end{bmatrix} \quad (6)$$

Conversely, the angular velocity of the vehicle frame can be obtained from Eq. (5) as

$$\omega_V = \begin{bmatrix} p \\ q \\ r \end{bmatrix} = T^{-1}\omega \quad (7)$$

where

$$T^{-1} = \begin{bmatrix} 1 & 0 & -\sin(\theta) \\ 0 & \cos(\phi) & \sin(\phi)\cos(\theta) \\ 0 & -\sin(\phi) & \cos(\phi)\cos(\theta) \end{bmatrix} \quad (8)$$

2.2 Dynamics

The translational motion equation under the influence of gravity force is defined as

$$f = m(\dot{V}_V + \omega_V \times V_V) + G \quad (9)$$

where $f = [f_x f_y f_z]^T$ is the translation force, m is the mass of the system, and G is the gravity force. Substituting Eqs. (4) and (7) into Eq. (9) yields

$$f = m\left(\begin{bmatrix} \dot{u} \\ \dot{v} \\ \dot{w} \end{bmatrix} + \begin{bmatrix} p \\ q \\ r \end{bmatrix} \times \begin{bmatrix} u \\ v \\ w \end{bmatrix}\right) + R^T \begin{bmatrix} 0 \\ 0 \\ -mg \end{bmatrix} \quad (10)$$

where g is the gravitational acceleration.

Solving Eq. (10) for $\dot{V}_V$ yields

$$\begin{bmatrix} \dot{u} \\ \dot{v} \\ \dot{w} \end{bmatrix} = \begin{bmatrix} rv - qw \\ pw - ru \\ qu - pv \end{bmatrix} + \begin{bmatrix} g\sin\theta \\ -g\cos\theta\sin\phi \\ -g\cos\theta\cos\phi \end{bmatrix} + \frac{1}{m}\begin{bmatrix} f_x \\ f_y \\ f_z \end{bmatrix} \quad (11)$$

Note that $f_x = f_y = 0$ and $f_z = f_T$ where f_T is the total thrust force since we have four rotors to control the elevation, roll, pitch, and yaw angles.

In the same way, the moment equation can be described as

$$M = I \cdot \dot{\omega}_V + \omega_V \times (I \cdot \omega_V) \quad (12)$$

where $M = \begin{bmatrix} \tau_\phi & \tau_\theta & \tau_\psi \end{bmatrix}^T$ is the moment force and I is the moment of the system, given as

$$I = \begin{bmatrix} I_{XX} & 0 & 0 \\ 0 & I_{YY} & 0 \\ 0 & 0 & I_{ZZ} \end{bmatrix} \quad (13)$$

where I_{XX}, I_{YY}, I_{ZZ} are the moment of inertia about the X,

Y, Z axes, respectively.

Substituting Eqs. (7) and (13) into Eq. (12) yields

$$M = \begin{bmatrix} I_{XX} & 0 & 0 \\ 0 & I_{YY} & 0 \\ 0 & 0 & I_{ZZ} \end{bmatrix} \begin{bmatrix} \dot{p} \\ \dot{q} \\ \dot{r} \end{bmatrix} + \begin{bmatrix} p \\ q \\ r \end{bmatrix} \times \left(\begin{bmatrix} I_{XX} & 0 & 0 \\ 0 & I_{YY} & 0 \\ 0 & 0 & I_{ZZ} \end{bmatrix} \begin{bmatrix} p \\ q \\ r \end{bmatrix} \right) \tag{14}$$

Rearranging Eq. (14) with respect to $\dot{\omega}_V$ yields

$$\begin{bmatrix} \dot{p} \\ \dot{q} \\ \dot{r} \end{bmatrix} = \begin{bmatrix} \frac{I_{YY} - I_{ZZ}}{I_{XX}} qr \\ \frac{I_{ZZ} - I_{XX}}{I_{YY}} pr \\ \frac{I_{XX} - I_{YY}}{I_{ZZ}} pq \end{bmatrix} + \begin{bmatrix} \frac{1}{I_{XX}} \tau_\phi \\ \frac{1}{I_{YY}} \tau_\theta \\ \frac{1}{I_{ZZ}} \tau_\psi \end{bmatrix} \tag{15}$$

It is convenient to represent dynamic Eqs. (11) and (15), specified for the vehicle frame, into a global frame through relationship Eq. (2). The dynamic equation in the global frame, assuming that the Coriolis terms and gyroscopic effects can be neglected, yields

$$\begin{aligned} m\ddot{x} &= f_T(\cos\phi \sin\theta \cos\psi + \sin\phi \sin\psi) \\ m\ddot{y} &= f_T(\cos\phi \sin\theta \sin\psi - \sin\phi \cos\psi) \\ m\ddot{z} &= f_T \cos\theta \cos\phi - mg \\ I_{xx}\ddot{\phi} &= \tau_\phi \\ I_{yy}\ddot{\theta} &= \tau_\theta \\ I_{zz}\ddot{\psi} &= \tau_\psi \end{aligned} \tag{16}$$

During hovering, the thrust force is assumed to be proportional to the square of propeller's rotational speed, that is,

$$F_i \approx \alpha_{thrust} w_i^2 \tag{17}$$

where α_{thrust} is the constant and w_i is propeller i's rotational speed. The drag force is assumed to be proportional to the square of the rotational speed of the propeller, that is,

$$D_i \approx \alpha_{drag} w_i^2 \tag{18}$$

where α_{drag} is the constant.

Although we have six variables to represent the system, we have only four inputs, making the quad-rotor an underactuated system. We regard the elevation$z$, roll, pitch, and yaw angles (ϕ, θ, ψ) as the control variables. Therefore, each force has the following relationship with the force produced by each rotor.

$$\begin{aligned} f_T &= F_F + F_B + F_R + F_L \\ \tau_\phi &= L(F_L - F_R) \\ \tau_\theta &= L(F_B - F_F) \\ \tau_\psi &= C(F_R + F_L - F_F - F_B) \end{aligned} \tag{19}$$

where f_T is the total thrust force;τ_ϕ, τ_θ, τ_ψ are the torque of the roll, pitch, and yaw angles, respectively; L is the distance from the center of mass of the system to the center of each rotor; and C is a constant factor.

3. Control Schemes

3.1 Linear Control

The angle of the quad-rotor system is regulated by controlling the velocity of each rotor. The direction of movement of the system is determined by combining the magnitudes of each rotor velocity. Although there are six variables for describing a quad-rotor system, there are only four actuators, which means that control of all six variables is difficult.

The linearized dynamics for the attitude control can be given from Eq. (16) as

$$\begin{aligned} m(\ddot{z} + g) &= f_T \\ I_{xx}\ddot{\phi} &= \tau_\phi \\ I_{yy}\ddot{\theta} &= \tau_\theta \\ I_{zz}\ddot{\psi} &= \tau_\psi \end{aligned} \tag{20}$$

Thus, basic movements such as reaching a certain altitude and hovering while adopting a specific attitude can be considered. The hovering motion is related to the control of the roll and pitch angles, and the attainment of altitude is related to the control of the thrust force. Since a quad-rotor system is a symmetrical structure, yaw angle control is not considered seriously in this case.

From the roll and pitch control inputs, the force input to each rotor can be determined. Each rotor force is described as

$$f = C_R u \tag{21}$$

where

$$f = \begin{bmatrix} F_F \\ F_B \\ F_R \\ F_L \end{bmatrix}, \; C_R = \begin{bmatrix} 1/4 & 0 & -\frac{1}{2L} & -\frac{1}{4C} \\ 1/4 & 0 & \frac{1}{2L} & -\frac{1}{4C} \\ 1/4 & -\frac{1}{2L} & 0 & \frac{1}{4C} \\ 1/4 & \frac{1}{2L} & 0 & \frac{1}{4C} \end{bmatrix},$$

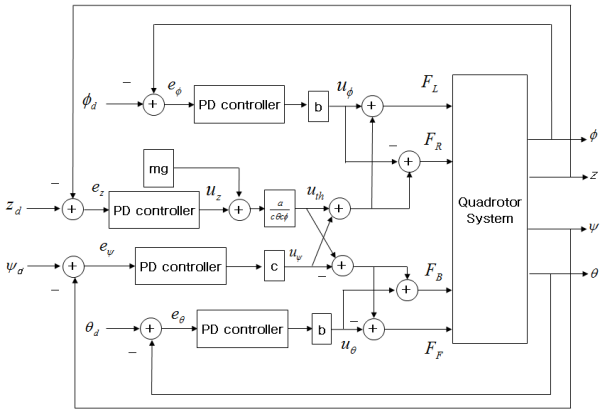

Figure 2. Control block diagram.

and

$$u = \begin{bmatrix} u_{th} \\ u_{\phi} \\ u_{\theta} \\ u_{\psi} \end{bmatrix}.$$

In this case, u_{th}, u_{ϕ}, u_{θ}, u_{ψ} are the control inputs for the thrust, and the roll, pitch, and yaw angles, respectively.

3.2 Simulation Studies

Based on the control block diagram shown in Figure 2, we performed a simulation study. We control the altitude and three angles.

The desired trajectories for the attitude control are given differently with respect to the time range.

i) $0 \sim 4$s: $z_d = 5m$, $\phi_d = 0$, $\theta_d = 0$, $\psi_d = 0$

ii) $4 \sim 10$s: $z_d = 5 + 3\sin(2\pi 4t)m$,

$$\phi_d = 0,\ \theta_d = 0,\ \psi_d = 0$$

iii) $10 \sim 15$s: $z_d = 5 + 3\sin(2\pi 0.25t)m$,

$$\phi_d = 0.1\sin(2\pi 0.5t),$$

$$\theta_d = 0,\ \psi_d = 0$$

Table 2 lists the controller gains. The attitude control performances are shown in Figure 3. We see that the quad-rotor system follows the desired trajectory well.

Table 2. Controller gains

	Roll, ϕ	Pitch, θ	Yaw, ψ	Altitude, z
k_p	10	10	10	100
k_d	4	4	4	40

Table 3. Specification of small quad rotor system

Variable	Value
Mass	0.95 kg
Length	0.5 m
Height	0.2 m
Maximum thrust	2 kg
MCU	ATMEGA 644 8-bit processor
Sensors	Accelerometer, gyro
Sampling time	4 ms

4. Design of Small Quad-Rotor System

Figure 4 shows the actual small quad-rotor system. The body frame is casted. As the control hardware, AVR is used rather than DSP to reduce the cost.

The sampling time is 4 ms. All of the hardware and sensors are located in the center of the unit. For angle detection, a gyro and an accelerometer are used.

Table 3 lists the specifications of the small quad rotor system. The total mass is 0.95 kg and the maximum thrust is 2 kg.

Figure 5 is an overall block diagram of the control hardware. The 8-bit microprocessor performs all of the calculations: control signals, sensor signals, and communication.

5. Practical Limitations

5.1 Computing Algorithms for Angles

To obtain the roll and pitch angles, a 3-axis gyro and 3-axis accelerometer are used. The following equations are used to obtain the roll and pitch angles from the accelerometer measurements.

$$\begin{aligned} \phi &= \tan^{-1}\left(\frac{a_x}{\sqrt{a_y^2 + a_z^2}}\right) \\ \theta &= \tan^{-1}\left(\frac{a_y}{\sqrt{a_x^2 + a_z^2}}\right) \end{aligned} \tag{22}$$

where a_x, a_y, a_z are the measured acceleration values for each axis as determined from the accelerometer.

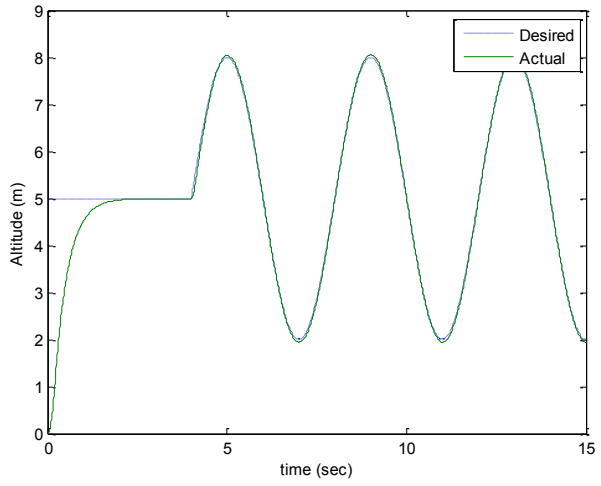

(a) Altitude

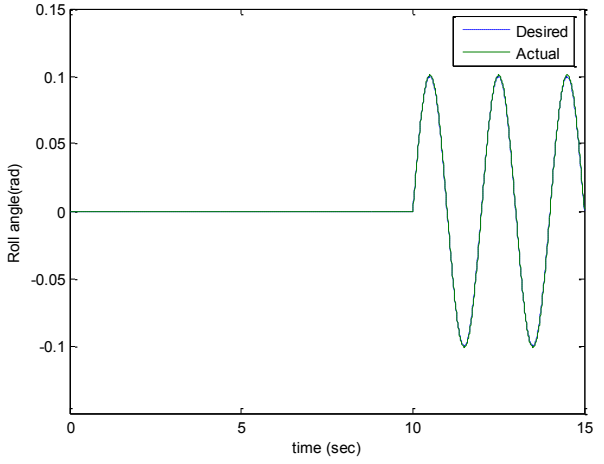

(b) Roll angle

Figure 3. Attitude control.

Figure 4. Small quad-rotor system.

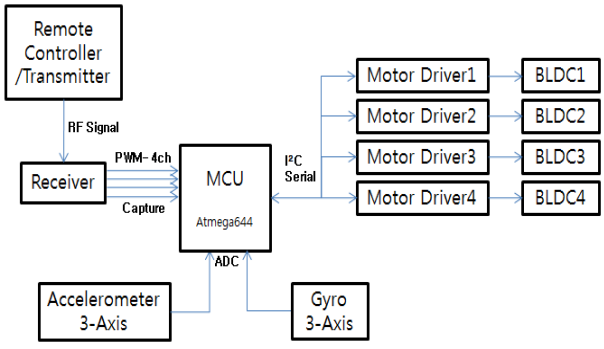

Figure 5. Overall block diagram of system.

Thus, computing Eq. (22) is a burden for an 8-bit processor, since $\tan^{-1}$ and $\sqrt{}$ operations require the math library and they are calculated based on the floating point data format. This leads to the computational limitation of the processor since the inherent processor cannot handle those computations within an acceptable sampling time. Therefore, the approximation of those mathematical operations is required to approximate the necessary mathematical functions.

5.1.1 Square Root Operation

The square operation can be approximated and obtained by applying Newton's method through several iterations. Eq. (23) defines the relationship of the square operation. Given value a, value b can be calculated as follows.

$$\begin{aligned} b &= sqrt(a), \\ b^2 - a &= 0 \end{aligned} \tag{23}$$

Newton's method is given as

$$x_{n+1} = x_n - \frac{f(x_n)}{f'(x_n)} \tag{24}$$

Reformulating Eq. (23) into Eq. (24) yields the update equation.

$$b_{n+1} = b_n - \frac{b_n^2 - a}{2b_n} \tag{25}$$

where n is the sequence.

Finally, the value of b can be obtained iteratively.

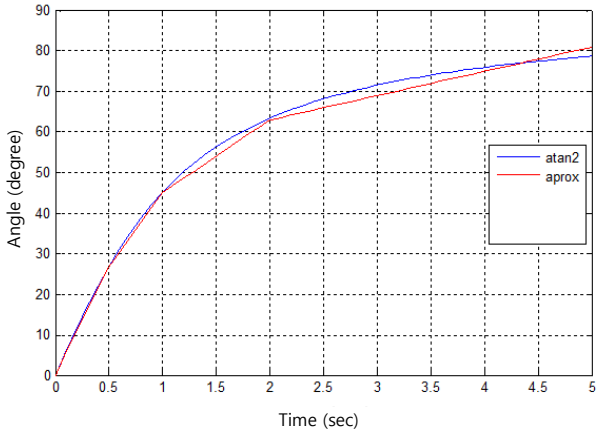

Figure 6. Approximation of $atan2$ function.

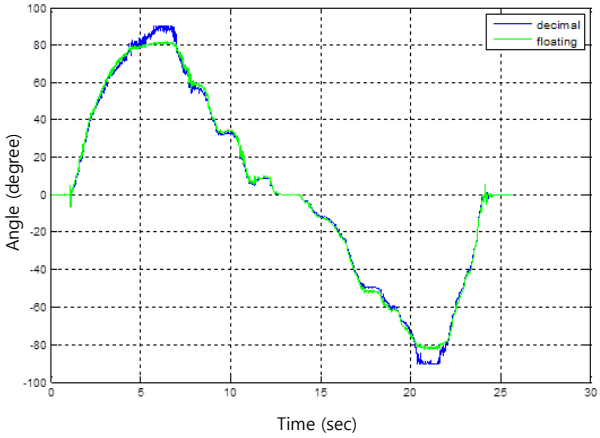

Figure 7. Test of approximation of $atan2$ function.

5.1.2 $\tan^{-1}$ Operation

For the $\tan^{-1}$ operation, a table lookup method is used to match the real values of $\tan^{-1}$ with several linear functions within the range of useful angles.

Although there are mismatch errors resulting from the approximation process, these errors are small and can be neglected for real applications. Figure 6 shows the approximation of the $atan2$ function within the range of $0° \sim 90°$ by four linear functions.

5.1.3 Integer Operation

Another consideration is the use of the integer operation rather than the floating point format for numerical calculations. For example, a typical IIR filter calculation can be performed as Eq. (26) for the floating point format that is not permitted by processors with low computational power. Therefore, the integer-based operations in Eq. (27) should be performed by accepting lower computing accuracy.

$$\mathrm{y[n+1]} = \mathrm{a1} * \mathrm{y[n]} + \mathrm{b1} * \mathrm{x[n]} + \mathrm{b2} * \mathrm{x[n-1]} \quad (26)$$

$$\mathrm{y[n+1]} = (\mathrm{a1} * \mathrm{y[n]} + \mathrm{b1} * \mathrm{x[n]} + \mathrm{b2} * \mathrm{x[n-1]})/10 \quad (27)$$

Within the useful range of angles, namely, from $0°$ to $\pm 90°$, the approximated integer operation is compared with the floating point operation shown in Figure 7. The two operations are similar except around $\pm 90°$ where there is a slight mismatch between the two operations.

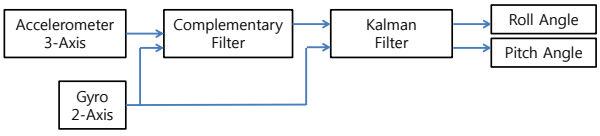

Figure 8. Two-stage filtering process.

5.2 Complementary Filtering Method

We measured the roll and pitch angles using an accelerometer and a gyro sensor. Since the accuracy of the sensors is poor due to the noisy environment, we applied two-stage filtering. The first-stage filtering involves the use of a complementary filter to maximize the filter characteristics. Then, the second stage filtering technique uses a Kalman filter after the complementary filter to suppress the effects of noise, as shown in Figure 8.

We designed filters that combined the two low-cost sensors: a gyro sensor and an accelerometer. We combine the two sensors as a complementary filter to obtain more accurate angle measurements. The complementary filter consists of a low-pass filter for the accelerometer and a high-pass filter for the gyro sensor. The filtered outputs are added together to estimate the value, as shown in Figure 9.

When the sensor transfer functions are given for the accelerometer as $H_a(s)$, and for the gyro sensor as $H_g(s)$, the complementary filter satisfies the following relationship:

$$H_a(s)F_a(s) + H_g(s)F_g(s) = 1, \quad (28)$$

where $F_a(s)$ and $F_g(s)$ are the transfer functions for the filters. If the sensor characteristics are unknown, we suggest the

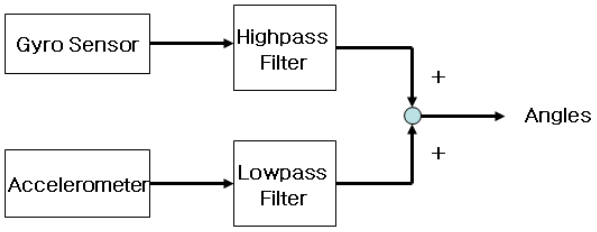

Figure 9. Complementary filter.

application of $H_a(s) = 1$ and $H_g(s) = 1$ for simplicity.

Then, each filter of $F_a(s)$, $F_g(s)$ can be simply designed as a first-order filter.

$$F_a(s) = \frac{1}{\lambda s + 1}, F_g(s) = \frac{\lambda s}{\lambda s + 1}, \tag{29}$$

where $F_a(s)$ is a low-pass filter, $F_g(s)$ is a high-pass filter, and λ is the time constant. The appropriate cutoff frequency for the low-pass and high-pass filters can be found by an empirical process. In our case, $\lambda = 0.77$ is obtained from the empirical studies.

5.3 Simplified Kalman Filter

The Kalman filter equation for the angle measurement is given by [21, 22]

$$\begin{aligned} x_{k+1} &= \begin{bmatrix} 1 & -dT \\ 0 & 1 \end{bmatrix} x_k + \begin{bmatrix} dT \\ 0 \end{bmatrix} u_k + w_k \\ y_k &= \begin{bmatrix} 1 & 0 \end{bmatrix} x_k + v_k \end{aligned} \tag{30}$$

where dT is the sampling time (4 ms),

$$\begin{aligned} x_k &= \begin{bmatrix} Angle\ predict \\ Gyro\ bias \end{bmatrix}; \\ y_k &= [Measured\_angle]; \\ u_k &= [Gyro\ rate]; \end{aligned}$$

and w_k and v_k are the process noise and measurement noise, respectively.

The conventional Kalman filter requires several repetitive steps to estimate states Eq. (31) to Eq. (35).

Time update:

$$\hat{x}_k^- = A\hat{x}_{k-1} + Bu_{k-1} \tag{31}$$

$$P_k^- = AP_{k-1}A^T + Q \tag{32}$$

Measurement update:

$$K_k = P_k^- H^T (HP_{k-1}H^T + R)^{-1} \tag{33}$$

$$\hat{x}_k = \hat{x}_k^- + K_k(z_k - H\hat{x}_k^-) \tag{34}$$

$$P_k = (I - K_k H)P_k^- \tag{35}$$

where Q and R are the covariance matrices of the process and measurement noises, respectively.

However, the computation of the Kalman filter is a considerable burden for an 8-bit microprocessor. Although the Kalman filtering method normally requires an iterative procedure to update the state correctly, a simplified version can be used. Instead of using all the steps of the Kalman filtering algorithm, a simplified process can be employed whereby the Kalman gain is fixed. In this case, the updates of Eqs. (32, 33, 35) are not required. Therefore, the form of the simplified Kalman filter algorithm will be as follows:

Time update :

$$\hat{x}_k^- = A\hat{x}_{k-1} + Bu_{k-1} \tag{36}$$

Measurement update :

$$\hat{x}_k = \hat{x}_k^- + K(z_k - H\hat{x}_k^-) \tag{37}$$

where the Kalman gain K is a fixed Kalman gain and $H = [1, 0]$.

5.4 Filtering Test

We conducted a filtering test based on the aforementioned simplified algorithms. The result of one typical filtering test is shown in Figure 10. The results of the single-stage and two-stage filter design technique are compared. The filtered signal, after being passed through the complementary filter, is compared with the signals output from the Kalman filter after the complementary filter. We can clearly see that the signals output from the two-stage filtering method, after being passed through the complementary and Kalman filters, are more stable.

5.5 Overall Hardware Structure

The signals obtained from the filtering algorithms were used in the control algorithms. Figure 11 shows the connection between the control and the filtering block diagram. The roll and pitch angles are measured by a gyro and an accelerometer, and those signals are fused with the complementary filter, for which the cutoff frequency is set to 1.3 Hz. Then, the signals are passed

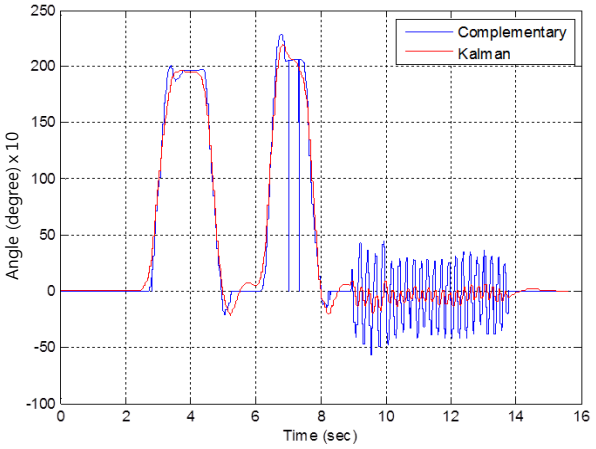

Figure 10. Filtered signals.

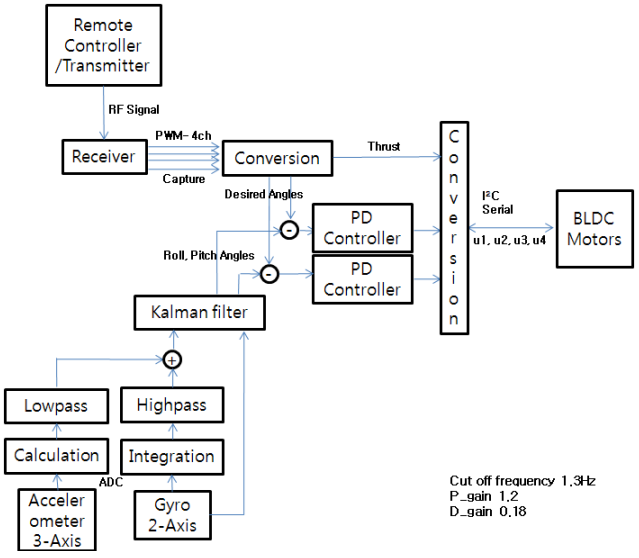

Figure 11. Control and filtering process.

through the Kalman filter.

The filtered signals are used for PD controllers and the PD gains are set to 1.2 and 0.18 for the proportional and derivative gain, respectively. Then, the control torque applied to each rotor is calculated by Eq. (19).

6. Experiments

6.1 Indoor Flying Task

After implementing the hardware and software under the aforementioned constraints, flying tests were conducted for real operations. Firstly, a flying test for the small quad-rotor system was performed inside a building to minimize disturbances such as that presented by wind.

Figure 12. Indoor flying demonstration.

Figure 12 shows a flying demonstration controlled by a joystick through a remote controller.

Another indoor flying test was conducted in a small space. Figure 13 illustrates an actual indoor flying task where the quad-rotor elevates from the floor and then lands on the floor. All of the trajectory commands are issued by the remote controller. The corresponding roll and pitch angle plots are shown in Figure 14. We can clearly see that the roll and pitch angles are well balanced. The oscillation errors are within about $\pm 5^{\circ}$.

6.2 Outdoor Flying Task

After adjusting the control parameters for stable flying in the indoor environment, the quad-rotor system was tested in an outdoor environment (on the roof of a building). Figure 15 illustrates the actual flying movement. The quad-rotor system was controlled by an operator.

7. Conclusion

We have presented the implementation of a small quad-rotor system under several practical constraints of minimizing the total cost. Changing the main control hardware from a DSP to an AVR limits the computational ability of the filtering and control algorithms. To satisfy the desired sampling time, the required mathematical functions are simplified and approximated. In addition, a simplified version of the Kalman filtering algorithm is presented and used for actual system control. Actual flying demonstrations in both indoor and outdoor environments con-

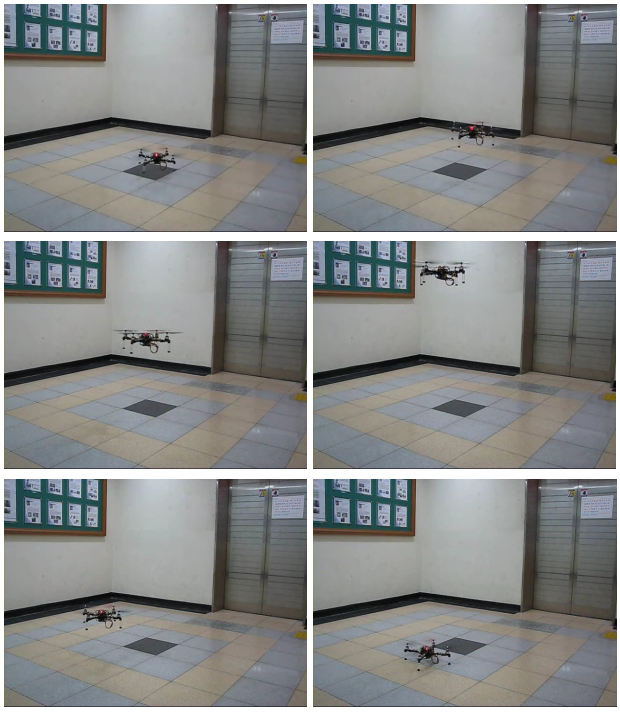

Figure 13. Flying control of small quad-rotor indoors.

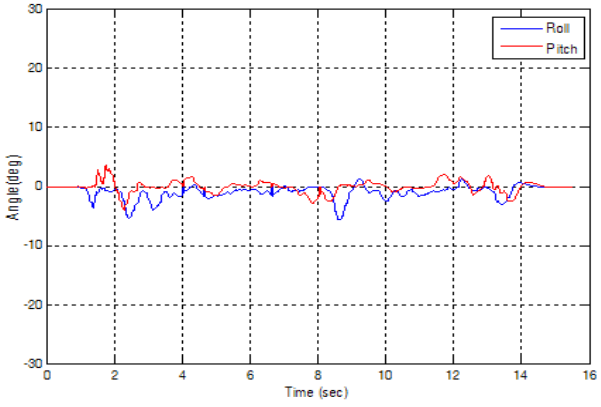

Figure 14. Roll and pitch angles for Figure 13.

firmed the functionality of the small quad-rotor system using approximated calculations for the algorithms.

Conflict of Interest

No potential conflict of interest relevant to this article was reported.

Figure 15. Flying control of small quad-rotor outdoors.

Acknowledgments

This research has been supported by Korea Research Foundation (KRF) through the general research program (2010-0024904) in Korea and the center for autonomous intelligent manipulation (AIM) for service robots of the Ministry of Knowledge Economy (MKE), Korea, under the Human Resources Development Program for Convergence Robot Specialists support program supervised by the National IT Industry Promotion Agency (NIPA) (NIPA-2013-H1502-13-1001).

References

[1] I. Tusseyeva, S. G. Kim, and Y. G. Kim, "3D global dynamic window approach for navigation of autonomous underwater vehicles," *International Journal of Fuzzy Logic and Intelligent Systems*, vol. 13, no. 2, pp. 91-99, Jun. 2013. http://dx.doi.org/10.5391/IJFIS.2013.13.2.91

[2] D. Y. Im and Y. J. Ryoo, "Development of steering actuator for unmanned vehicle based on magnetic marker," *Journal of Korean Institute of Intelligent Systems*, vol. 19, no. 3, pp. 375-378, Jun. 2009. http://dx.doi.org/10.5391/JKIIS.2009.19.3.375

[3] S. W. Jeon and S. Jung, "Localization and control of an outdoor mobile robot based on an estimator with sensor fusion," *Journal of Institute of Embedded Engineering of Korea*, vol. 4, no. 2, pp. 69-78, Jun. 2009.

[4] D. W. Kim, Y. Igor, E. S. Kang, and S. Jung, "Design and control of an omni-directional cleaning robot based on landmarks," *Journal of Korean Institute of Intelligent*

Systems, vol. 23, no. 2, pp. 100-106, Apr. 2013. http://dx.doi.org/10.5391/JKIIS.2013.23.2.100

[5] D. Y. Yun and S. H. Kim, "A design of fire monitoring system based on unmaned helicopter and sensor network," *Journal of Korean Institute of Intelligent Systems*, vol. 17, no. 2, pp. 173-178, Apr. 2007. http://dx.doi.org/10.5391/JKIIS.2007.17.2.173

[6] I. Y. Eom and S. Jung, "Intelligent force control application of an autonomous helicopter system," *Journal of Institute of Embedded Engineering of Korea*, vol. 6, no. 5, pp. 303-309, Oct. 2011.

[7] M. H. Kim, J. B. Park, H. J. Lee, D. B. Cha, and Y. H. Joo, "A decentralized control technique for experimental nonlinear helicopter systems," *Journal of Korean Institute of Intelligent Systems*, vol. 12, no. 1, pp. 80-84, Feb. 2002.

[8] T. G. Amaral, M. M. Crisóstomo, and V. F. Pires, "Helicopter motion control using adaptive neuro-fuzzy inference controller," in *Proceedings of the 28th Annual Conference of the IEEE Industrial Electronics Society*, Sevilla, Spain, November 5-8, 2002, pp. 2090-2095. http://dx.doi.org/10.1109/IECON.2002.1185295

[9] E. Altuğ, J. P. Ostrowski, and R. Mahony, "Control of a quadrotor helicopter using visual feedback," in *Proceedings of the IEEE International Conference on Robotics and Automation* Washington, DC, May 11-15, 2002, pp. 72-77. http://dx.doi.org/10.1109/ROBOT.2002.1013341

[10] P. Castillo, A. Dzul, and R. Lozano, "Real-time stabilization and tracking of a four-rotor mini rotorcraft," *IEEE Transactions on Control Systems Technology*, vol. 12, no. 4, pp. 510-516, Jul. 2004. http://dx.doi.org/10.1109/TCST.2004.825052

[11] R. Xu and Ü. Özgner, "Sliding mode control of a quadrotor helicopter," in *Proceedings of the 45th IEEE Conference on Decision and Control*, San Diego, CA, December 13-15, 2006, pp. 4957-4962. http://dx.doi.org/10.1109/CDC.2006.377588

[12] B. Erginer and E. Altuğ, "Modeling and PD control of a quadrotor VTOL vehicle," in *Proceedings of the IEEE Intelligent Vehicles Symposium*, Istanbul, Turkey, June 13-15, 2007, pp. 894-899. http://dx.doi.org/10.1109/IVS.2007.4290230

[13] Y. Bouktir, M. Haddad, and T. Chettibi, "Trajectory planning for a quadrotor helicopter," in *Proceedings of the Mediterranean Conference on Control and Automation*, Ajaccio-Corsica, France, June 25-27, 2008, pp. 1258-1263. http://dx.doi.org/10.1109/MED.2008.4602025

[14] A. Das, K. Subbarao, and F. Lewis, "Dynamic inversion with zero-dynamics stabilisation for quadrotor control," *IET Control Theory and Applications*, vol. 3, no. 3, pp. 303-314, Mar. 2009. http://dx.doi.org/10.1049/iet-cta:20080002

[15] T. Dierks and S. Jagannathan, "Output feedback control of a quadrotor UAV using neural networks," *IEEE Transactions on Neural Networks*, vol. 21, no. 1, pp. 50-66, Jan. 2010. http://dx.doi.org/10.1109/TNN.2009.2034145

[16] A. Tayebi and S. McGilvray, "Attitude stabilization of a VTOL quadrotor aircraft," *IEEE Transactions on Control Systems Technology*, vol. 14, no. 3, pp. 562-571, May 2006. http://dx.doi.org/10.1109/TCST.2006.872519

[17] S. Bouabdallah and R. Siegwart, "Full control of a quadrotor," in *IEEE/RSJ International Conference on Intelligent Robots and Systems*, San Diego, CA, October 29-November 2, 2007, pp. 153-158. http://dx.doi.org/10.1109/IROS.2007.4399042

[18] R. Zhang, X. Wang, and K. Y. Cai, "Quadrotor aircraft control without velocity measurements," in *Proceedings of the 48th IEEE Conference on Decision and Control held jointly with 2009 28th Chinese Control Conference*, Shanghai, China, December 15-18, 2009, pp. 5213-5218. http://dx.doi.org/10.1109/CDC.2009.5400463

[19] H. Huang, G. M. Hoffmann, S. L. Waslander, and C. J. Tomlin, "Aerodynamics and control of autonomous quadrotor helicopters in aggressive maneuvering," in *Proceedings of the IEEE International Conference on Robotics and Automation*, Kobe, Japan, May 12-17, 2009, pp. 3277-3282. http://dx.doi.org/10.1109/ROBOT.2009.5152561

[20] S. H. Jeong, M. K. Lee, and S. Jung, "Calibration and control of rotor actuation of flymobile by force measurements," in *Proceedings of the 7th International Conference on Ubiquitous Robots and Ambient Intelligence*, Busan, Korea, November 24-27, 2010, pp. 395-398

[21] S. H. Jeong and S. Jung, "Implementation of low cost small quadrotor system," in *Korea Robotics Society Annual Conference*, Jeonju, Korea, July, 2011, pp. 15-18.

[22] M. Achtelik, Z. Tianguang, K. Kuhnlenz, and M. Buss, "Visual tracking and control of a quadcopter using a stereo camera system and inertial sensors," in *International Conference on Mechatronics and Automation*, Changchun, China, August 9-12, 2009, pp. 2863-2869. http://dx.doi.org/10.1109/ICMA.2009.5246421

[23] B. Herissé, T. Hamel, R. Mahony, and F. X. Russotto, "Landing a VTOL Unmanned aerial vehicle on a moving platform using optical flow," *IEEE Transactions on Robotics*, vol. 28, no. 1, pp. 77-89, Feb. 2012. http://dx.doi.org/10.1109/TRO.2011.2163435

[24] M. Schwager, B. J. Julian, M. Angermann, and D. Rus, "Eyes in the sky: decentralized control for the deployment of robotic camera networks," *Proceedings of the IEEE*, vol. 99, no. 9, pp. 1541-1561, Sep. 2011. http://dx.doi.org/10.1109/JPROC.2011.2158377

Seung Ho Jeong received the B.S. and M.S degrees in Mechatronics Engineering from Chungnam National University, Daejeon, Korea in 2010 and 2012, respectively. In his graduate school, he developed and controlled a quadrotor system. After graduation, he has been a researcher at LIG Nex1. His research interests include the development and control of unmanned vehicle systems. He is a member of Institute of Control, Robotics, and Systems in Korea.

Seul Jung received the B.S. degree in Electrical & Computer Engineering from Wayne State University, MI, USA and the M.S & Ph.D. degrees from University of California, Davis, USA, both in Electrical & Computer Engineering. He has joined the Department of Mechatronics Engineering at the Chungnam National University, Daejeon, Korea from 1997. While at Chungnam National University, he has engaged in research and teaching in the areas of robotics, intelligent systems, digital control, and signal processing. He has focused his efforts in robotics and intelligent control systems. He developed a graduate program in intelligent control and robot control, and established an Intelligent Systems and Emotional Engineering (I.S.E.E) Laboratory for both theoretical and experimental studies. The Lab focuses on the validation of theories by experimental studies of Mechatronics systems. His robotics research includes robot force control, multi-arm coordination, neural network applications to robotics, and robot education. More recently, he has been engaged in outreach program of introducing robots to young students from local schools. He has been a member in the IEEE Robotics and Automation Society, IEEE Control System Society, IEEE Industrial Electronics Society, Institute of Control, Robotics, and Systems, Korean Institute of Intelligent Systems, Institute of Electronics Engineers of Korea, Korean Institute of Electrical Engineers, and Institute of Embedded Engineering of Korea. He has served as a program committee member in many international conferences. He also has been an executive office member in the Institute of Control, Robotics, and Systems (ICROS) and Korean Institute of Intelligent Systems(KIIS) in Korea.